Influence of phosphorus on the growth and the photoluminescence properties of Si-NCs formed in P-doped SiO/SiO 2 multilayers

Fatme Trad, Alaa E Giba, Xavier Devaux, Mathieu Stoffel, Denis Zhigunov, Alexandre Bouché, Sébastien Geiskopf, Rémi Demoulin, Philippe Pareige, Etienne Talbot, et al.

Influence of phosphorus on the growth and the photoluminescence properties of Si-NCs formed in P-doped SiO/SiO_2 multilayers

F. Trad,[a] Alaa E. Giba,[a,b] X. Devaux,[a] M. Stoffel,[a] D. Zhigunov,[c] A. Bouché,[a] S. Geiskopf,[a] R. Demoulin,[d] P. Pareige,[d] E. Talbot,[d] M. Vergnat,[a] H. Rinnert*[a]

[a] *Université de Lorraine, CNRS, Institut Jean Lamour, F-54000 Nancy, France*

[b] *National Institute of Laser Enhanced Sciences, Cairo University, Giza 12613, Egypt*

[c] *Skolkovo Institute of Science and Technology, Bolshoy Boulevard 30, bld. 1, 121205 Moscow, Russia*

[d] *Normandie Univ., UNIROUEN, INSA Rouen, CNRS, Groupe de Physique des Matériaux, 76000 Rouen, France*

Abstract

This work reports on the influence of phosphorous atoms on the phase separation process and optical properties of silicon nanocrystals (Si-NCs) embedded in phosphorus doped SiO/SiO_2 multilayers. Doped SiO/SiO_2 multilayers with different P contents have been prepared by co-evaporation and subsequently annealed at different temperatures up to 1100 °C. The sample structure and the localization of P atoms were both studied at the nanoscale by scanning transmission electron microscopy and atom probe tomography. It is found that P incorporation modifies the mechanism of Si-NC growth by promoting the phase separation during the post-growth-annealing step, leading to nanocrystals formation at lower annealing temperatures as

compared to undoped Si-NCs. Hence, the maximum of Si-NC related photoluminescence (PL) intensity is achieved for annealing temperatures lower than 900 °C. It is also demonstrated that the Si-NCs mean size increases in the presence of P, which is accompanied by a redshift of the Si-NC related emission. The influence of the phosphorus content on the PL properties is studied using both room temperature and low temperature measurements. It is shown that for a P content lower than about 0.1 at. %, P atoms contribute to significantly improve the PL intensity. This effect is attributed to the P-induced-reduction of the number of non-radiative defects at the interface between Si-NCs and SiO_2 matrix, which is discussed in comparison with hydrogen passivation of Si-NCs. In contrast, for increasing P contents, the PL intensity strongly decreases, which is explained by the growth of Si-NCs reaching sizes that are too large to ensure quantum confinement and to the localization of P atoms inside Si-NCs.

Keywords: Si nanocrystals; Phosphorous; Doping; Phase separation; Nanoscale analysis

Introduction

During the last decades, silicon nanocrystals (Si-NCs) have attracted a great deal of attention in various fields like optoelectronics, sensors, plasmonics, and solar cells.[1, 2, 3, 4] Both the quantum confinement effect and the tunable size-dependent bandgap open great opportunities to effectively control the optical absorption and emission of Si-based devices. Doping Si-NCs with either negatively and/or positively charged impurities is a promising route for tailoring their optical and electrical properties. Si-NCs could be efficiently used in all Si-based tandem solar cells, in which n- and p- type layers of Si-NCs can be obtained. Moreover, co-doping is also a promising approach to induce electronic levels in the bandgap, which could provide novel optical

emission bands in Si-based materials. Thus, efficient sub-bandgap emission in co-doped Si-NCs dispersed in a colloidal solution[5,6] or prepared by nonthermal plasma synthesis[7] was demonstrated. Although some calculations predicted high formation energies for impurities in semiconductor nanocrystals, [8] experimental works demonstrated that P atoms can be preferentially localized in Si-NCs rather than in the surrounding silicon oxide matrix. [9] These observations are further in good agreement with other calculations. [10,11] Despite many efforts to introduce efficient dopants into Si-NCs and to investigate the doping-induced electronic properties, many questions still exist, in particular related to the effective generation of free carriers.[12,13] The electronic activation of the inserted impurities is often studied through absorption or photoluminescence (PL) measurements. The existence of free carriers in Si-NCs has been successfully deduced from absorption in the infrared range for heavily P-doped Si-NCs.[14,15] Moreover, the activation of dopants in Si-NCs can be argued by the loss of PL emission from Si-NCs, which may be interpreted as a signature of an Auger effect.[15,16] However, as suggested in the literature, the PL quenching could also originate from defects induced by doping.[17] König et al. claimed that P is unlikely to provide electrons to Si-NCs embedded in SiO_2 because P atoms found inside Si-NCs are almost exclusively located in interstitial states.[18] The PL quenching is then due to deep levels induced by P in the surrounding SiO_x shell. In addition, a blueshift of the Si-NCs related PL can be interpreted by a preferential quenching of luminescence of the bigger Si-NCs, which are more likely to contain dopants.[15,16] A precise knowledge of the localization of dopants is a key issue to improve the understanding of the doping induced optoelectronic properties. In case of Si-NCs embedded in a SiO_2 matrix, dopants could be localized in the nanocrystal core, at their surface or in the surrounding matrix. Because of the difficulty to experimentally localize the dopant at the nanoscale, the experimental results

dedicated to the localization of dopants are still scarce. Among the potential experimental methods, atom probe tomography (APT) is an efficient way to localize dopants. Such a technique has given evidence that P atoms can be inserted into Si-NCs.[19,20] Using APT to investigate P-doped Si-NCs embedded in a SiO_2 matrix, Gnaser et al. have reported that around 20 % of P atoms are localized inside Si-NCs, whereas 30 % reside at the interface and 50 % remain in the matrix.[21] In addition to the localization of dopants, the potential modification of the growth process and the size of the Si-NCs induced by the impurities are of primary importance to interpret the optical properties of layers containing Si-NCs and dopants. A correlation between the accurate location of dopants and the optoelectronic properties could strongly help to reach a better understanding of the doping at the nanoscale.

In this paper, we report on the influence of P on the optical properties of Si-NCs formed in SiO/SiO_2 multilayers in relation with the growth of the nanocrystals, the defects and the localization of dopants. The optical properties are analyzed by temperature-dependent PL spectroscopy. Structural and chemical analyses at the nanoscale were carried out by scanning transmission electron microscopy (STEM), STEM electron energy loss spectroscopy (STEM-EELS) and APT. We shed light on the strong modification of the phase separation process in Si-rich SiO_2 layers, induced by the softening of the oxide and suboxide layers, which is of primary importance to interpret the PL properties of Si-NCs. Our results indicate that depending on the P content, P atoms lead to a significant improvement of the Si-NCs PL properties or to the quenching of the Si-NCs emission.

Experimental

P-doped (SiO/SiO_2):P multilayers were obtained by alternating the deposition of SiO and SiO_2 compounds provided by two electron-beam guns on Si(001) substrates held at room temperature. Materials for evaporation are high purity (99.99 %) SiO and SiO_2 grains with a typical size of 2 to 4 mm. The deposition rates of SiO and SiO_2, equal to 0.1 nm/s were controlled by quartz microbalances. P atoms were supplied by a GaP decomposition source, maintained at a controlled temperature during all the deposition process, hence leading to the incorporation of P atoms in both SiO and SiO_2 layers. The P content was controlled by the temperature of the GaP cell.[22] As the P content cannot be accurately measured by the quartz microbalance during deposition, the P concentration in the layer was measured after deposition by energy dispersive x-ray spectroscopy and atom probe tomography. A calibration curve was then established giving the correspondence between the GaP cell temperature and the global P content in the film. The following exponential dependence was determined: $\log(C_P) = 16.1 - 1.78\times10^4/T$, where C_P is the P concentration given in atomic percentage and T is the cell temperature given in Kelvin. The P atomic concentration was varied from 5×10^{-5} to 2.5 at. %, corresponding to cell temperatures ranging from 600 °C to 860 °C. As-deposited samples were amorphous. The samples were then post-grown annealed in a rapid thermal annealing furnace at different temperatures up to 1100 °C for 5 minutes under N_2 flow (200 sccm). Some samples were subjected to a hydrogen passivation process, carried out at 500 °C during 5 min under a flow of forming gas N_2 (90%) / H_2 (10%). STEM and STEM-EELS experiments were carried out using a JEOL ARM 200 F probe corrected with a cold field emission gun. EELS spectrum images (SI) were recorded with a Gatan GIF quantum ER filter. To avoid any phase precipitation due to electron beam damages, experiments were performed at 80 kV with a probe current of about 50 pA for EELS spectrum images. Two EELS-SI were simultaneously recorded for the

low-loss part containing the zero-loss and for the core-loss which allows advanced data post processing like energy drift corrections and multiple scattering corrections. The spectra were recorded with an electron beam having a half convergence angle of 24 mrad for a half collection angle of 56 mrad with an energy dispersion of 0.05 eV/channel and a pixel time of 0.005 s. SI were recorded with a spatial sampling of about 0.2×0.2 nm^2/pixel. A multivariate statistical analysis software was used to improve the quality of the STEM-EELS data by de-noising the core-loss SI. Low-loss spectra were processed by zero-loss extraction and Fourier-log deconvolution for multiple scattering corrections. To draw chemical maps, multiple linear least square fitting was applied on Si_L and P_L signals. Due to the overlapping of Si_L and P_L edges, and to separate chemical states of Si (Si^0 and Si^{IV}), reference spectra were recorded on pure Si, on pure thermal silica grown on a Si wafer and on SiP_2. The reference spectra were extracted from SI recorded on lamellae with the same thickness, and with the same STEM and spectrometer parameters as that of the samples under study. For TEM and STEM observations, lamellas thinned up to $t/\lambda < 0.8$ (ratio between the thickness t and the electron mean free path λ) were prepared by focused ion beam (FIB) using a FEI Helios Nanolab 600i dual beam microscope. During FIB operation, the samples were capped by a pure carbon thin layer followed by a Pt-C layer to protect the sample during the first steps of the lamella extraction. After FIB milling, the lamellae were stored in vacuum to prevent oxidation. The 3D high resolution structural and chemical analysis at atomic scale was also conducted by APT. Experiments were carried out using a laser-assisted wide-angle tomographic atom probe (LAWATAP, Cameca) with a femtosecond UV pulsed laser (λ=343nm, 350 fs, 33 nJ). The analysis was performed in a high-vacuum chamber under 10^{-10} mbar at 80 K. Tip shaped samples were prepared using a ThermoScientific plasma FIB Helios G4 XCe. APT data treatments and 3D reconstruction were

obtained using GPM3Dsoft software. The steady state PL was measured using the 325 nm He-Cd laser as an excitation. The PL signal was collected by a monochromator equipped with a 600 grooves/mm grating and measured by a cooled photomultiplier tube operating in the visible-NIR range. The spectra were corrected for the system response.

Results and discussion

(SiO/SiO_2):P multilayers were prepared using SiO and SiO_2 thicknesses equal to 2.5 and 5 nm, respectively. The number of bilayers is 20, hence a total film thickness of 150 nm for all samples is considered in this study. Figure 1 shows cross-sectional STEM-EELS images for (SiO/SiO_2):P multilayers annealed at 1100 °C having a phosphorus content of 7.8×10^{-3} at. % (Fig. 1(a)) and 4×10^{-1} at. % (Figs. 1 (b)-(e)). Si atoms in a Si matrix (Si^0), Si atoms in silica (Si^{4+}), as well as phosphorous atoms are shown in red, green and blue colors, respectively. Fig. 1 (a) shows that Si-NCs are formed in the deposited SiO layers and that the size distribution seems to be rather narrow, as expected for such multilayers structures.[23,24] Moreover, this analysis shows that the multilayer structure is preserved for such a low P content. However, for larger P contents, as high as 4×10^{-1} at. %, the multilayer structure can hardly be distinguished and some disorder is evident, as shown in Figs. 1(b)-(c) by mapping the same sample area for visualization of Si atoms in Si-NCs and Si in the surrounding SiO_2 matrix, correspondingly. To detect clearly P atoms by STEM EELS analysis, several samples with different P concentrations have been carefully studied. For P concentrations below 6×10^{-2} at. %, it is not possible to extract any significant signature of P atoms from the EELS spectra, which corresponds probably to the detection limit of the technique. However, starting from a concentration of 6×10^{-2} at. % (images not shown here), P atoms can be detected. They are almost randomly localized in the multilayer

structure: in the amorphous SiO_2 matrix, close to the Si-NCs/SiO_2 interface or inside Si-NCs. The situation changes for higher P contents. Indeed, for a P concentration of 4×10^{-1} at. %, P atoms are preferentially localized inside Si-NCs, as evident from the superposition of Si^0 and P related maps shown in Fig. 1(e). However, as this view corresponds to a 2D projection, the localization of P atoms at the interface cannot be fully excluded, even if elemental profiles across Si-NCs do not show the double peak characteristic of core-shell like microstructure with an over concentration of phosphorus at the SiO_2/Si-NCs interface. To verify these results and to get a better understanding of the localization of P atoms, APT experiments were carried out.

Figure 2 shows the APT results obtained for (SiO/SiO_2):P multilayers annealed at 1100 °C in case of an undoped sample as compared with three samples with different P concentrations equal to 7.8×10^{-3}, 6.10^{-2} and 4×10^{-1} at. %. Cross section volumes extracted from the 3D reconstruction for the different samples revealing the position of Si and P atoms in $21\times21\times3$ nm^3 boxes are represented in Figs. 2(a-d). It should be noted that P atoms cannot be detected in the sample containing 7.8×10^{-3} at. % of P which is below the detection limit of P by APT in our samples. For all samples, Si-NCs are clearly identified as Si atom dense spots. The average diameter and size distribution of Si-NCs are almost independent of the P concentration up to a value of 6×10^{-2} at. %. For a P concentration of 4×10^{-1} at. % (see Fig. 2(d)), Si-NCs are significantly larger. The size distributions shown in Figs.2 (e)-(f) clearly indicate that the average size increases from 2.5 nm to 3.1 nm when the P concentration increases from 7.8×10^{-3} at. %. to 4×10^{-1} at. %. The expected mean size, controlled by the SiO thickness is 2.5 nm, which is indeed observed for undoped multilayers and for P contents below or equal to 6×10^{-2} at. %. In addition, the size distribution for the highest P concentration becomes broader, suggesting that the size of the Si-NCs is not fully controlled by the SiO_2 barrier layers in presence of a high quantity of

impurities. APT allows determining the localization of P atoms for concentrations higher or equal to 6×10^{-2} at. %. For this concentration, the 2D map (Fig. 2 (c)) clearly indicates that P atoms can be found in the SiO_2 matrix and that some P atoms are localized inside Si-NCs or at the matrix/Si-NCs interface. P atoms seem to be almost randomly localized. On the contrary, for higher P contents, i.e. 0.4 at. % of P in average, the sample is characterized by a preferential localization of P atoms inside Si-NCs, as shown in Fig. 2(d). From the APT analysis, the fraction of P atoms remaining in the SiO_2 matrix can be estimated to about 40 %. To determine the accurate localization and concentration of P atoms inside Si-NCs, an erosion profile was performed on more than one hundred of Si-NCs and the characteristic profile is shown in Figure 3.

The erosion profile highlights the evolution of the composition of each species from the Si-NCs core to the SiO_2 matrix.[25] The position zero on the x-axis corresponds to the interface between Si-NC and SiO_2 matrix. Concerning P atoms, the shape of the erosion profile shows a significant increase of the P composition in the core of Si-NCs, unambiguously demonstrating that most of P atoms are indeed localized inside Si-NCs, reaching a raw concentration as high as 8 at. %. It must be mentioned that a high concentration of O atoms is also measured inside the Si-NCs. This observation is due to the local magnification effect occurring during APT analyses of multi-phased systems.[26] A correction of this measurement artefact (see ref. 27) allows to estimate a P concentration of 11 to 12 at. % inside the Si-NCs, far beyond the solubility limit of P in bulk Si. Even if the erosion profile does not show any sign of self-purification effect, which is characterized by a P composition peak at the Si-NC/SiO_2 interface, it cannot be excluded that some P atoms are localized at the Si-NCs surface. Moreover the interface between the Si-NC and the surrounding matrix is not sharp. As shown on the erosion profile, the evolution of the Si

concentration from the minimum value to the maximum value extends over 2 nm. The spatial evolution of the P content from almost zero in SiO_2 up to the highest value of about 8 at.% in Si-NC also extends over 2 nm which suggests that some P atoms are located at the interface between Si-NCs and the SiO_2 matrix.

The above presented structural and chemical study at the nanoscale shows that the introduction of P impurities in the SiO/SiO_2 multilayer strongly affects the growth of Si-NCs for P concentrations higher than around 0.1 at.%. For low P concentrations, i.e. below 0.1 at. %, the Si-NC mean size is controlled by the SiO_2 barrier layers and the multilayer structure leads to a relatively narrow Si-NC size distribution. P atoms are almost randomly localized in the matrix, inside Si-NCs or at the SiO_2/Si-NC interface. The distribution of the number of P atoms per Si-NC is broad and approximately one third of nanocrystals contains 1 P atom. Beyond this concentration, the Si-NC mean size is no longer controlled by the multilayer structure, and the size distribution becomes broader. Moreover, P atoms are preferentially localized inside Si-NCs and P concentrations as high as 10 at. % can be found in some Si-NCs. These results indicate that, while thermodynamics is not favorable to the location of P atoms inside Si-NCs, high concentrations of P atoms can be nevertheless inserted inside Si-NCs. The driving force that controls the localization of dopants and the enriched distribution of P inside Si-NCs is probably the solubility limit of phosphorus, which is very different in Si and in SiO_2. The impurity redistribution at the SiO_2/Si interface is well known and if boron segregates preferentially in SiO_2, both arsenic and phosphorus are known to accumulate at the Si surface. In particular it has been shown that the phosphorus concentration can be four orders of magnitude higher in Si than in SiO_2 at the SiO_2/Si interface after an annealing treatment at 1100 °C. [28] For the weakest P concentration used in our study, the P content in the multilayer is assumed to be lower than the

solubility limit of P in SiO_2 which explains an almost random localization of P in the layer. For higher P concentrations, phosphorus moves to Si, where the solubility limit is higher. It is worth noting that alloying at the nanoscale has not been observed in this study, while for higher P contents, the formation of SiP_2 nanocrystals inside a SiO_2 matrix has been reported.[29] For P concentrations larger than 0.1 at.%, the Si-NCs size increase and size distribution can be interpreted by a softening of the SiO_2 matrix induced by P impurities, as already suggested.[30] Our results are in good agreement with the P-induced Si-NCs size increase from 4 to 8 nm obtained from the phase separation in P-doped silicon-rich silicon oxide produced by co-sputtering with a P concentration of 0.5 at.%.[31] Moreover, the P-induced softening effect probably leads to an increase of the diffusion length of P atoms in the matrix and contributes to a higher concentration of P atoms inside Si-NCs.

The influence of P atoms on the optical properties of Si-NCs was studied by PL spectroscopy. PL measurements were carried out at room temperature on intrinsic multilayers and those containing P atoms for different annealing temperatures and different P concentrations. Figure 4(a) shows the dependence of the PL signal with the annealing temperature for intrinsic multilayers. For the as-deposited sample and the sample annealed at 700 °C, no significant PL is observed. For samples annealed at temperatures between 900 °C and 1000 °C, a very weak and broad PL is observed, which is a signature of amorphous Si nanoclusters formation.[32] The PL band intensity significantly increases with the annealing temperature, reaching the highest intensity for an annealing temperature of 1100 °C. This broad PL band, extending from 1.2 eV to 1.9 eV is attributed to the recombination of electrons and holes confined in Si-NCs. Fig. 4(b) shows the dependence of the PL signal with the annealing temperature for the (SiO/SiO_2):P multilayer containing 4×10^{-1} at.% of P. The introduction of P atoms in the multilayers leads to a

drastic change of the dependence of the PL emission of Si-NCs with the annealing temperature. Indeed, the PL intensity of Si-NCs starts to be intense already after an annealing temperature as low as 900 °C, and the highest PL intensity is observed for an annealing temperature of 1000 °C, i.e. 100 °C below the optimal annealing temperature for the undoped sample. Furthermore, it must be noted that the PL intensity characteristic of this optimal annealing is slightly higher that the highest PL shown by the intrinsic layer. However, the comparison of the PL intensity of both samples annealed at 1100 °C indicates a strong decrease of the PL intensity for the samples containing P atoms, by a factor close to 10. To get a better understanding of the optimal annealing temperature, i.e. the annealing temperature leading to the highest Si-NCs PL intensity, we have analyzed the annealing temperature dependence of the PL for multilayers with different P contents. Fig. 4(c) shows the optimal annealing temperature as a function of the P concentration. For P concentrations lower than 10^{-2} at. %, the optimal annealing temperature is almost unchanged, within the accuracy of the measurements, taking into account that samples were annealed at different temperatures with a step of 50 °C. For higher P contents, a decrease of the optimal annealing temperature is unambiguously induced by P doping. For a P concentration of 3.5 at. %, the optimal annealing temperature reaches a value as low as 800 °C. This can be explained by the P-induced softening of the matrix suggested above, which leads to the reduction of the thermal budget requested for the phase separation and crystallization processes followed by the formation of optically active Si-NCs.

Fig. 5(a) shows the normalized room temperature photoluminescence spectra of (SiO/SiO_2):P samples annealed at 1100 °C for different P concentrations. A P-induced PL redshift is clearly observed. Fig. 5(b) shows the PL energy which corresponds to the PL peak maximum as a function of the P content. For P contents up to 2×10^{-2} at. %, the PL energy slightly

decreases. However, for higher P, contents a pronounced redshift is observed from about 1.55 eV for the undoped and weekly doped layers to 1.42 eV for the sample doped with 1.1 at. % of P. A spectral shift could be interpreted by the activation of dopants inside Si-NCs. A P-induced PL blueshift was indeed explained by a preferential doping of the largest Si-NCs, which were assumed to be quenched by the Auger effect.[15,16] The observed PL spectral shift obtained with our samples cannot be interpreted by a preferential activation of dopants inside largest Si-NCs, but rather is due to the P-induced increase of the Si-NCs size and the associated weakening of the quantum confinement effect. Indeed, the PL redshift occurs concomitantly with the increase of the Si-NCs size for P contents higher than 0.1 at. %, as demonstrated by the microstructural study.

Fig. 5(b) also displays the dependence of the Si-NCs PL peak intensity with the P concentration. The PL intensity increases with P concentrations up to about 0.2 at.% and then decreases for higher concentrations until quenching occurs. Understanding the behavior of the PL intensity with the P content is not straightforward and should be considered in light of the P-induced growth modifications. A similar P dependence of the PL intensity has been reported, attributing the PL intensity increase to a reduction of the density of P_b centers at the interface between Si-NCs and SiO_2.[15] The interfacial defects act as non-radiative pathways and the decrease of their density would then result in a higher PL intensity in comparison with the undoped sample. However, another hypothesis could be raised to account for the increase of the PL intensity. As P promotes the phase separation, the addition of P could lead to an increase of the Si-NCs density, which is however not observed.

To investigate more into details the Si-NCs related PL intensity increase, low temperature PL measurements and passivation annealing treatments were carried out. Figure 6 shows the PL

spectra measured at 50 K, normalized to the peak at around 1.6 eV, for different P contents. The PL spectra are characterized by two peaks. The contribution at about 1.6 eV is due to the recombination of charge carriers confined in Si-NCs. This peak is slightly blueshifted as compared to the measurements at room temperature, which is well known and can be explained by the temperature dependence of the Si bandgap.[33,34] The second peak at around 1 eV is observed for our samples only at temperatures below about 150 K, and its intensity is a decreasing function of the temperature. This peak is obtained for both undoped and doped samples, which indicates that this PL band is not due to P-induced radiative defects or electronic levels. Moreover, being normalized to the confined charge carriers peak, this near-infrared contribution is a decreasing function of the P content. It is worth mentioning that Fujii et al. have reported a similar PL band emission at low temperatures from Si-NCs embedded in a SiO_2 matrix for undoped, B-doped or P-doped layers.[35,36,37] The origin of this sub-band is referred to the recombination of charge carriers trapped at the interfacial P_b centers, at the interface between Si-NCs and the SiO_2 matrix. A P_b center is the dominant electrically-active defect at the Si-SiO_2 interface, which introduces energy levels in the band-gap of SiO_2 and participates in the trapping and de-trapping of charge carriers.[38] The clear decrease of this defect-related contribution with increasing P contents shown in Fig. 6, strongly suggests that P insertion leads to a decrease of the number of P_b centers, which then contributes to the increase of the Si-NC related PL intensity shown in Fig. 5(b). The reduction of the number of interfacial defects could be attributed to the P-induced reduction of strain at the Si-NC/matrix interface during the cooling and/or annealing treatments.

To further study the role of P on P_b centers, both undoped and doped multilayers have been subjected to a passivation treatment, consisting of an annealing at 500 °C during 5 min

under forming gas. Figure 7 shows the low temperature PL spectra of an undoped multilayer annealed at 1100 °C prior to and after a passivation treatment. It can be observed that the P_b center-related defect band at ~1 eV is completely suppressed while the Si-NCs related PL is strongly enhanced after the passivation treatment, which leads to a decreasing number of P_b centers. This observation highlights the high efficiency of the passivation treatment. The inset of Fig. 7 shows the PL intensity of passivated Si-NCs as a function of the P content. It clearly appears that the PL intensity is a continuously decreasing function of the P concentration, which partially contradicts the evolution shown in Fig. 5 (b) for unpassivated Si-NCs. The reason for that is concerned with the fact, that Si-NCs prepared without any passivation treatment are characterized by the presence of P_b centers which limit their PL intensity. On the contrary, for hydrogen-passivated samples, defects are almost all suppressed and the presence of P atoms do not contribute, in that case, to an increase of the PL intensity. Our results suggest that P atoms contribute to the increase of the PL intensity only for layers containing defect centers. We believe that the mechanisms leading to an increase of the PL intensity, induced by forming gas passivation or P doping, are different. While H_2 molecules contained in a forming gas reduce the number of P_b centers after their formation during the annealing treatments at 1100 °C, the introduction of P atoms probably limits their formation because of the P-induced modification and softening of the SiO_x matrix. It can then be concluded that the introduction of P in passivated multilayers hence mainly contributes to decrease the PL intensity of Si-NCs. Two hypotheses may be put forward to explain the P induced Si-NC PL quenching. The first one is concerned with a non-radiative Auger recombination process, assuming that P atoms are active, while the second one is concerned with deep defect states providing efficient pathways for non-radiative charge carrier recombination. For the former, P is considered as a dopant, located in

substitutional states while for the later, P is considered to be in interstitial states or at the surface of the nanocrystals. Unfortunately, if the structural and chemical studies at the nanoscale are highly efficient to localize P atoms, the distinction between substitutional or interstitial sites is not achievable. If P atoms are in substitution and are electrically active, plasmons are expected to appear. Infrared absorption spectroscopy (results not shown here) measurements have been carried out in the 400-8000 cm^{-1} range and no absorption band has been observed, hence suggesting that no plasmonic related absorption occurs, which is however expected for the highest P concentration used in this work. In addition, it is demonstrated that P atoms play a significant role on the size distribution, inducing an increase of the mean size and an associated decrease of the quantum confined carriers related PL. Furthermore, as highlighted by APT and STEM-EELS analyses, some P atoms are expected to be localized at the interface between Si-NCs and SiO_2 matrix, where they may act as non-radiative centers. The small size of these nanocrystals embedded in a matrix and their high surface to volume ratio may not be favorable to the collective oscillation of free carriers or to an efficient doping.

Conclusions

(SiO/SiO_2):P multilayers with different P contents were prepared by co-evaporation of successive layers of SiO and SiO_2 from e-beam guns and P atoms were supplied by a GaP decomposition source. The optical properties were studied and compared with structural and chemical analysis at the nanoscale. The introduction of P atoms is shown to play a significant role on the phase separation and on the growth of Si-NCs within the SiO layers. P atoms induce a softening of the matrix leading to: i) the formation of highly luminescent Si-NCs at lower

annealing temperatures in comparison with undoped samples; ii) a PL redshift induced by a decrease of the SiO_2 barrier effect and a subsequent formation of Si-NCs with larger sizes; iii) an increase of the PL intensity induced by a decrease of non-radiative defects at the Si-NCs/SiO_2 interface for average P concentrations below 0.5 at.%, iv) a PL quenching induced not only by Si-NCs having sizes beyond the size limit for quantum confinement but also by P induced defects which may arise from the insertion of P inside Si-NCs. It is worth mentioning that, from the application point of view, P-doping of SiO/SiO_2 multilayers is of clear interest since the PL intensity can be strongly increased and the annealing temperature needed to reach a high PL intensity can be significantly reduced.

Author contributions

A.E.G.: investigation, optical properties, RTA process; S.G.: investigation, optical properties; F. Trad, D. Zhigunov, M. Stoffel: investigation, optical and structural properties; X.D.: investigation, TEM, STEM-EELS; R.D., P. P., E.T: investigation, atom probe tomography ; A.B.: growth of samples, technical support; M.V.: supervision, growth of layers; H.R.: supervision, photoluminescence, writing, original draft; AEG, D.Z., M.S., X.D., R.D., E.T., M.V., H.R. discussed the results and contributed to the manuscript.

Conflicts of interest

There are no conflicts of interest to declare.

Acknowledgements:

The authors acknowledge the ANR project DONNA (ANR-18-CE09-0034) and the French PIA project "Lorraine Université d'Excellence" reference no. ANR-15IDEX-04-LUE support. D.Z. gratefully acknowledges the support from the "Make Our Planet Great Again" short-stay program.

References

1 F. Priolo, T. Gregorkiewicz, M. Galli andT. F. Krauss, *Nat. Nanotechnol.*, 2014, **9**, 19–32.

2 J. L. Frieiro, J. López-Vidrier, O. Blázquez, D. Yazıcıoğlu, S. Gutsch, J. Valenta, S. Hernández, M. Zacharias and B. Garrido, *J. Appl. Phys.*, 2019, **126**, 144501.

3 C. M. Gonzalez and J. G. C. Veinot, *J. Mater. Chem. C*, 2016, **4**, 4836-4846.

4 M. C. Beard, K. P. Knutsen, P. Yu, J. M. Luther, Q. Song, W. K. Metzger, R. J. Ellingson and A. J. Nozik, *Nano Lett.*, 2007, **7**, 2506–2512.

5 Y. Hori, S. Kano, H. Sugimoto, K. Imakita, M. Fujii, *Nano Lett.*, 2016, **16**, 2615−2620.

6 M. Fujii, H. Sugimoto and K. Imakita, *Nanotechnology*, 2016, **27**, 262001.

7 R. Limpens, G. F. Pach and N. R. Neale, *Chem. Mater.*, 2019, **31**, 4426-4435.

8 G. M. Dalpian and J. R. Chelikowsky, *Phys. Rev. Lett.*, 2006, **96**, 226802.

9 M. Perego, G. Seguini, E. Arduca, J. Frascaroli, D. De Salvador, M. Mastromatteo, A. Carnera, G. Nicotra, M. Scuderi, C. Spinella, G. Impellizzeri, C. Lenardie and E. Napolitani, *Nanoscale*, 2015, **7**, 14469.

10 A. Carvahlo 1, S. Öberg, M. Barroso, M. J. Rayson, and P. Briddonand , *Phys. Status Solidi A*, 2012, **209**, 1847-1850.

11 R. Guerra and S. Ossicini, *J. Am. Chem. Soc*., 2014, **136**, 4404−4409.

12 E. Arduca and M. Perego, *Mater. Sci. in Semic. Process.*, 2017, **62**, 156-170.

13 B. L. Oliva-Chatelain, T. M. Ticich andA. R. Barron, *Nanoscale*, 2016, **8**, 1733–1745.

14 D. J. Rowe, J. S. Jeong, K. A. Mkhoyan and U. R. Kortshagen, *Nano Lett.*, 2013, **13**, 1317-1322.

15 A. Mimura, M. Fujii, S. Hayashi, D. Kovalev and F. Koch, *Phys. Rev. B*, 2000, **62**, 12625-12627.

16 S. Gutsch, A. M. Hartel, D. Hiller, N. Zakharov, P. Werner and M. Zacharias, *Appl. Phys. Lett.*, 2012, **100**, 233115.

17 D. Hiller, J. López-Vidrier, S. Gutsch, M. Zacharias, K. Nomoto and D. König, *Sci. Rep.*, 2017, **7**, 863.

18 D. König, S. Gutsch, H. Gnaser, M. Wahl, M. Kopnarski, J. Göttlicher, R. Steininger, M. Zacharias and D. Hiller, *Sci. Rep.*, 2015, **5**, 09702.

19 R. Khelifi, D. Mathiot, R. Gupta, D. Muller, M. Roussel and S. Duguay, *Appl. Phys. Lett.*, 2013, **102**, 013116.

20 R. Demoulin, M. Roussel, S. Duguay, D. Muller, D. Mathiot, P. Pareige and E. Talbot, *J. Phys. Chem. C*, 2019, **123**, 7381-7389.

21 H. Gnaser, S. Gutsch, M. Wahl, R. Schiller, M. Kopnarski, D. Hiller and M. Zacharias, *J. Appl. Phys.*, 2015, **115**, 034304.

22 G. Lippert, H. J. Osten, D. Krüger, P. Gaworzewski and K. Eberl, *Appl. Phys. Lett.*, 1995, **66**, 3197-3199.

23 M. Zacharias, J. Heitmann, R. Scholz, U. Kahler, M. Schmidt, J. Blasing, *Appl. Phys. Lett.*, 2002, **80**, 661-663.

24 O. Jambois, H. Rinnert, X. Devaux and M. Vergnat, *J. Appl. Phys.*, 2005, **98**, 46105.

25 *Atom probe tomography: put theory into practice*, ed. W. Lefebvre-Ulrikson, Academic Press, London, 2016.

26 F. Vurpillot, A. Bostel, and D. Blavette, *Appl. Phys. Lett.*, 2000, **76**, 3127-3129.

27 E. Talbot, R. Lardé, F. Gourbilleau, C. Dufour and P. Pareige, *EPL*, 2009, **87,** 26004.

28 K. Sakamoto, K. Nishi, F. Ichikawa and S. Ushio, *J. Appl. Phys.*, 1987, **61**, 1553

29 S. Geiskopf, M. Stoffel, X. Devaux, E. André, C. Carteret, A. Bouché, M. Vergnat and H. Rinnert, *J. Phys. Chem. C*, 2020, **124**, 7973–7978.

30 K. Sumida, K. Ninomiya, M. Fujii, K. Fujio, S. Hayashi, M. Kodama and H. Ohta, *J. Appl. Phys.*, 2007, **101**, 033504.

31 X. J. Hao, E. C. Cho, G. Scardera, E. Bellet-Amalric, D. Bellet, Y.S. Shen, S. Huang, Y.D. Huang, G. Conibeer and M.A. Green, *Thin Solid Films*, 2009, **517**, 5646-5652.

32 D. M. Zhigunov, V.N. Seminogov, V. Yu Timoshenko, V. I. Sokolov, V. N. Glebov, A. M. Malyutin, N. E. Maslova, O. A. Shalygina, S. A. Dyakov, A. S. Akhmanov, V. Ya Panchenko, and P. K. Kashkarov, *Physica E: Low Dimens. Syst. Nanostruct.*, 2009, **41**, 1006-1009.

33 J. Heitmann, F. Müller, L. Yi, M. Zacharias, D. Kovalev and F. Eichhorn, *Phys. Rev. B*, 2004, **69**, 195309.

34 H. Rinnert, O. Jambois and M. Vergnat, *J. Appl. Phys.*, 2009, **106**, 023501.

35 M. Fujii, S. Hayashi and K. Yamamoto, *J. Appl. Phys.*, 1998, **83**, 7953-7957.

36 S. Takeoka, M. Fujii and S. Hayashi, *Phys. Rev. B*, 2000, **62**, 16820-16825.

37 M. Fujii, A. Mimura, S. Hayashi and K. Yamamoto, *Appl. Phys. Lett.*, 1999, **75**, 184-186.

38 F. Li and A. Nathan, *CCD Image Sensors in Deep-Ultraviolet: Degradation Behavior and Damage Mechanisms*, Springer Berlin Heidelberg, 2006.

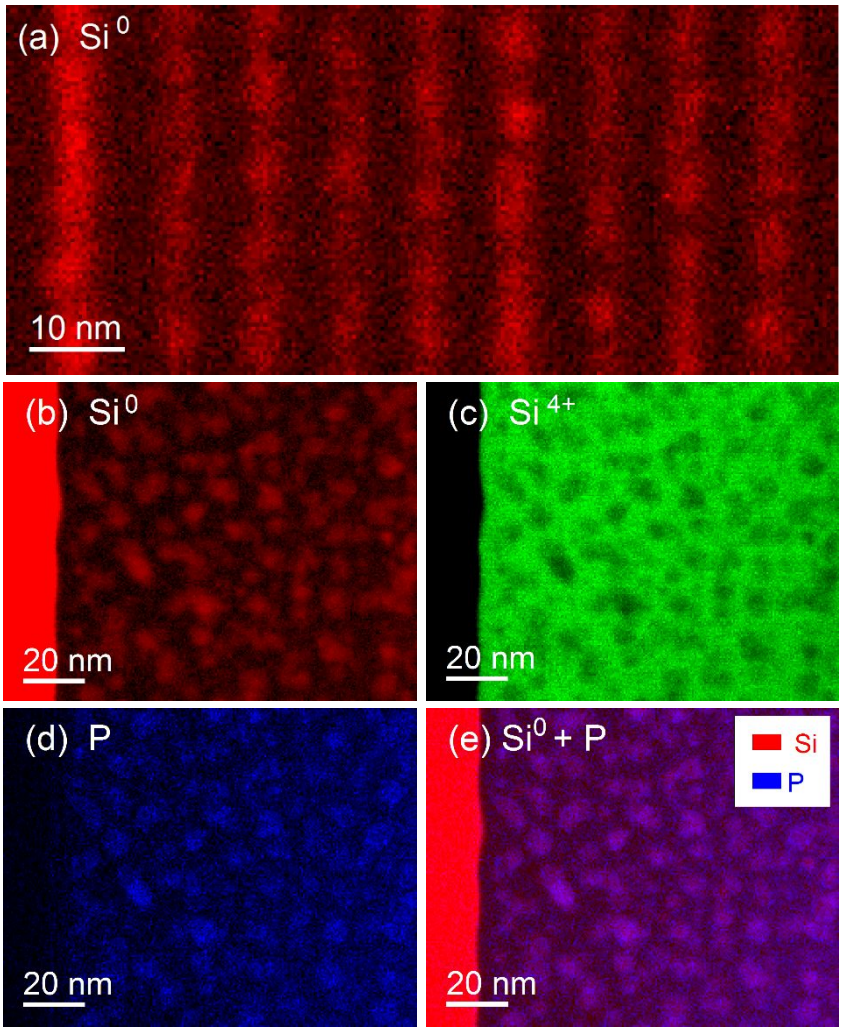

Fig. 1. STEM-EELS mapping for (SiO/SiO_2):P multilayers annealed at 1100 °C with a phosphorus content of (a) 7.8×10^{-3} at.%. and of (b-e) 4×10^{-1} at.%. Atoms of silicon in a Si environment, of silicon in SiO_2 and of phosphorous are shown in red, green and blue colors, respectively. (e) shows the superposition of (b) and (d).

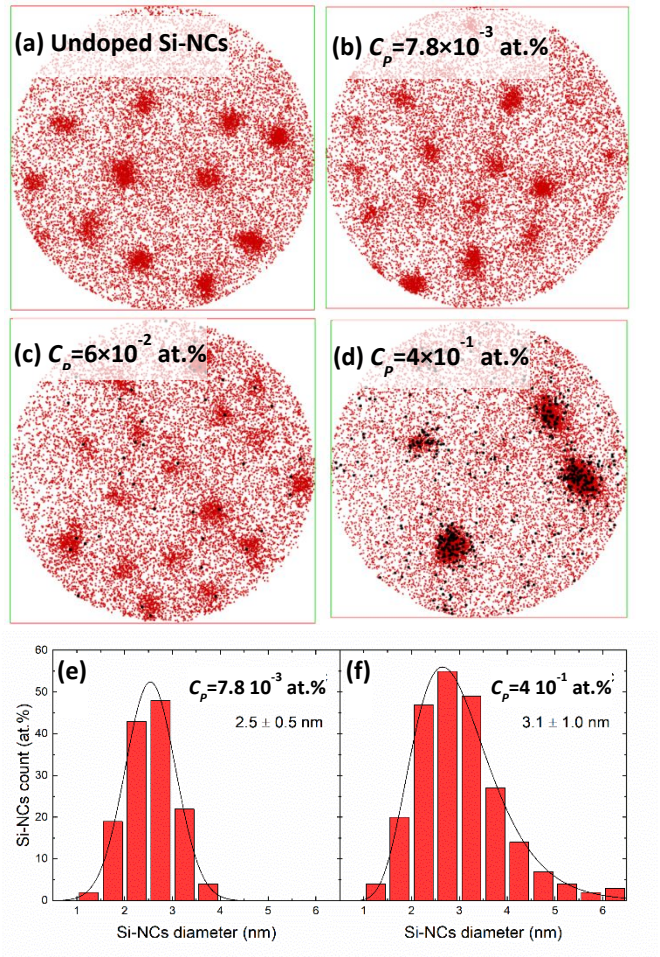

Fig. 2. 2D slice view (21 × 21 × 3 nm^3) taken from the 3D reconstructed volume showing both Si (red points) and P (black points) atoms for (SiO/SiO$_2$):P multilayers annealed at 1100 °C with (a) C_P=0 at.%, (b) C_P=7.8×10^{-3} at.%, (c) C_P=6×10^{-2} at.% and (d) C_P=4×10^{-1} at.%. Lower panel shows size dispersion of Si-NCs obtained from (SiO/SiO$_2$):P multilayer with (e) C_P=7.8×10^{-3} at.%, and (f) C_P=4×10^{-1} at.%, respectively.

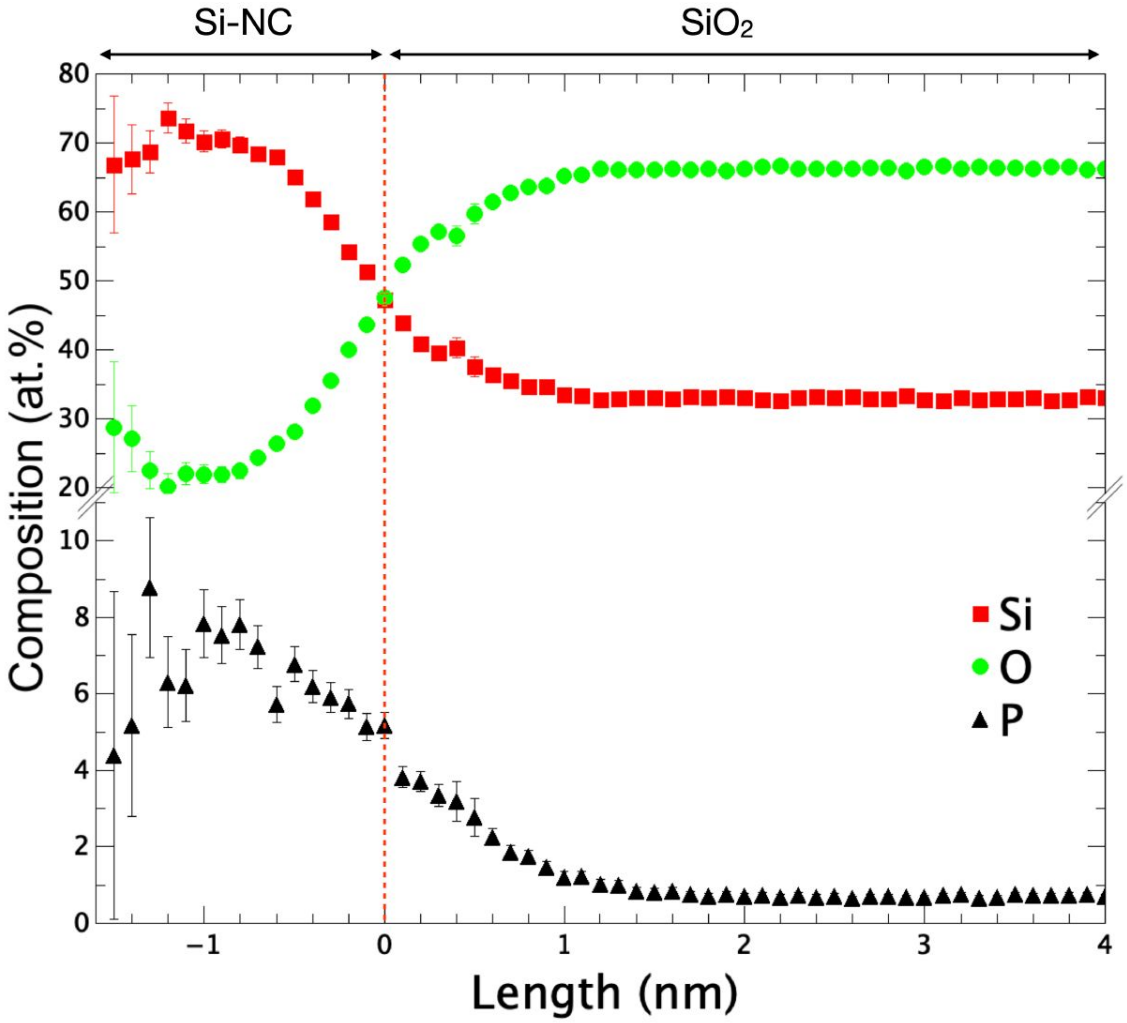

Fig.3. Erosion profile close to a Si-NC obtained by APT analysis for a multilayer annealed at 1100 °C with C_P=4.10^{-1} at.%. The zero position corresponds to the Si-NC/SiO_2 interface.

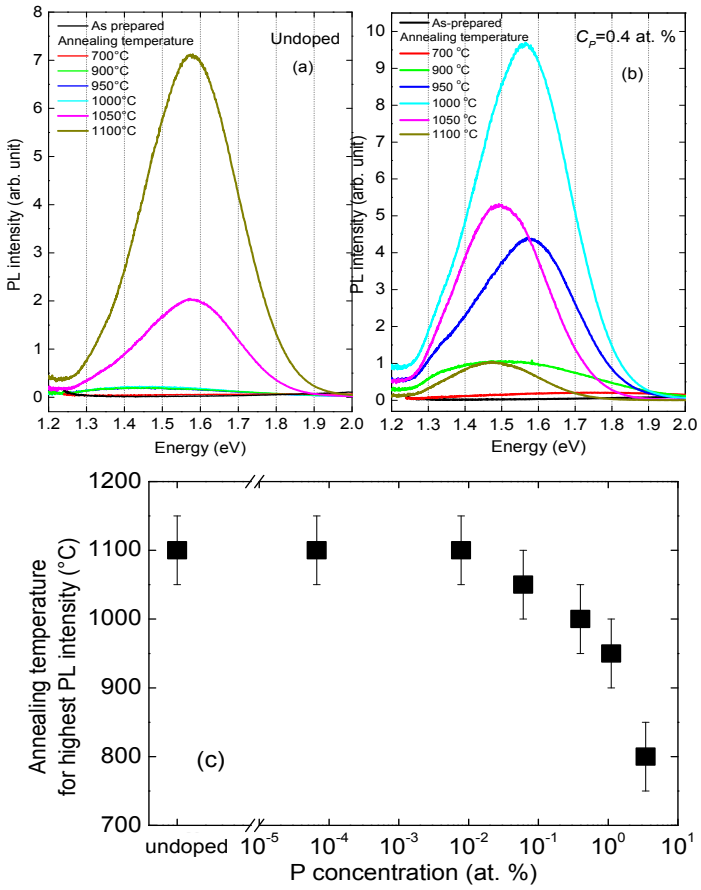

Fig.4. Room temperature photoluminescence spectra of samples annealed at different temperatures for (a) undoped SiO/SiO_2 and (b) (SiO/SiO_2):P with $C_P=4.10^{-1}$ at.%. (c) Dependence of the optimal annealing temperature with P content.

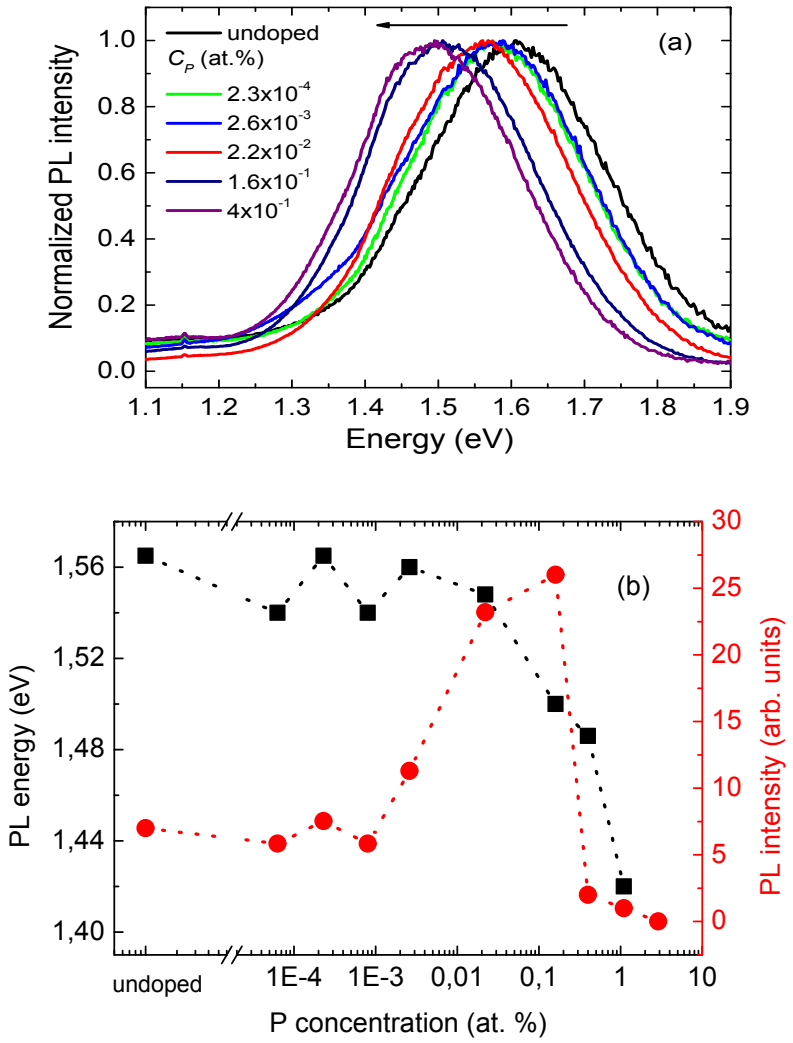

Fig.5. (a) Normalized room temperature photoluminescence of (SiO/SiO$_2$):P samples annealed at 1100 °C for different P concentrations; (b) Dependence of the PL peak energy and intensity with the P content.

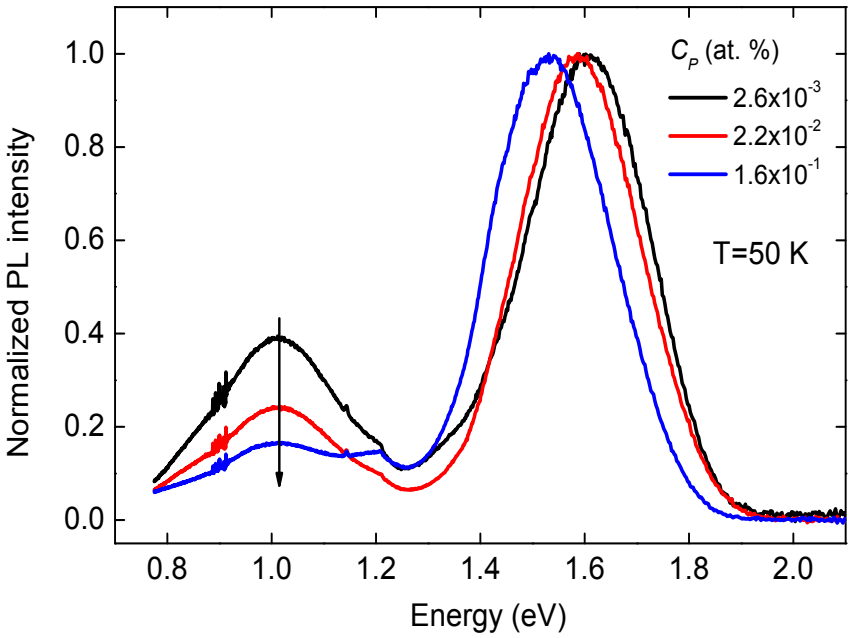

Fig. 6. Low temperature PL spectra for (SiO/SiO_2):P multilayers with different P concentrations. The spectra are normalized with respect to the peak at ~1.6 eV.

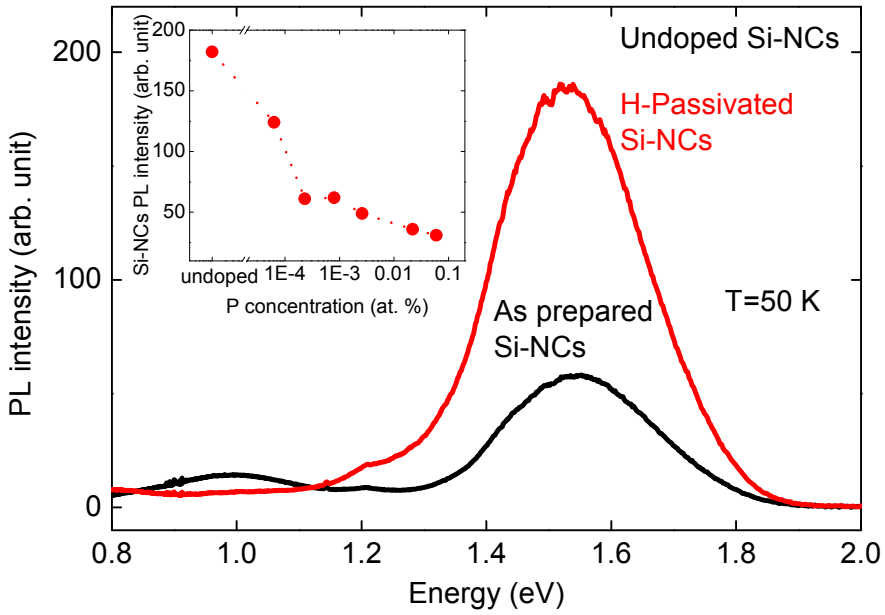

Fig. 7. PL spectra at 50 K of undoped SiO/SiO_2 multilayers annealed at 1100 °C with or without a passivation treatment. The inset shows the PL peak intensity of hydrogen passivated Si-NCs as a function of the P concentration.

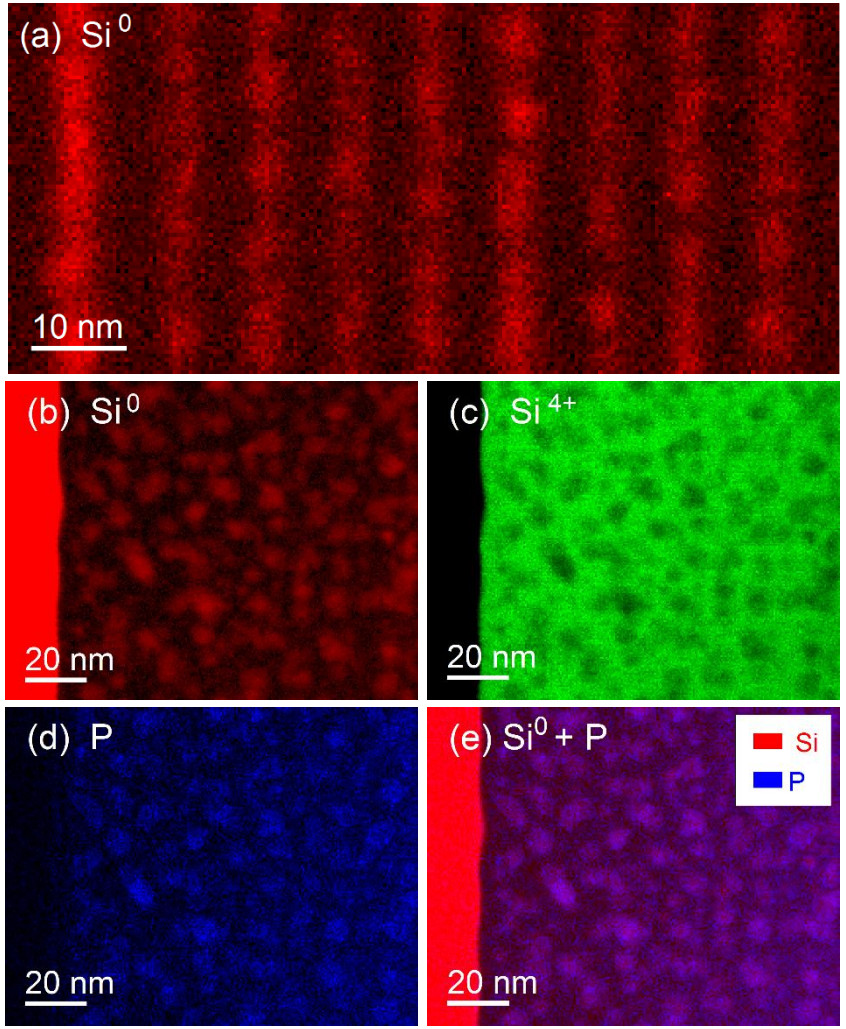
(a) Si 0
10 nm
(b) Si 0
20 nm
(c) Si 4+
20 nm
(d) P
20 nm
(e) Si0 + P
Si
P
20 nm

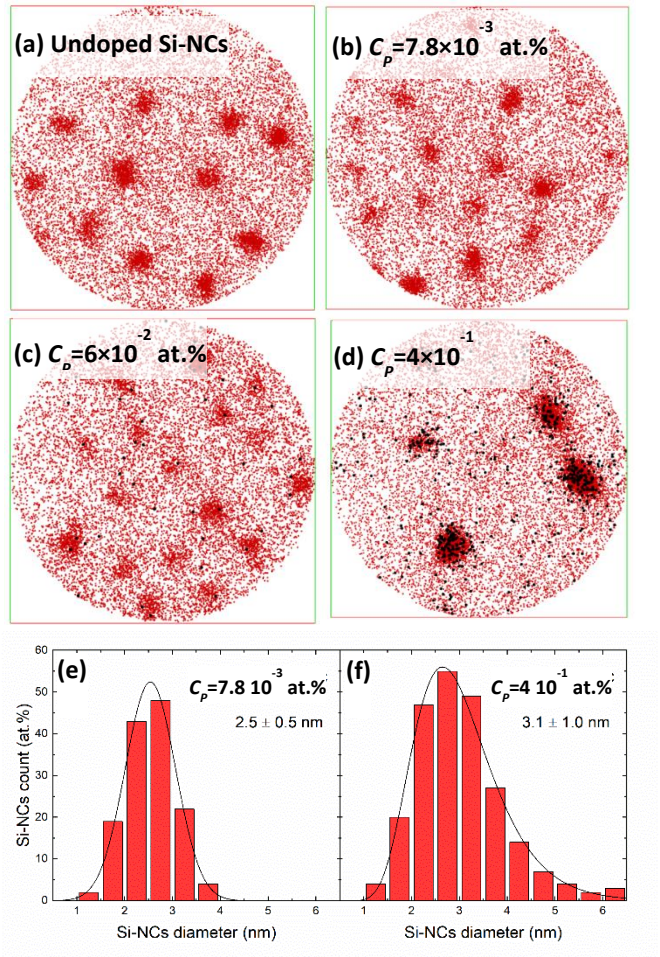
(a) Undoped Si-NCs
(b) C_P=7.8×10^{-3} at.%
(c) C_P=6×10^{-2} at.%
(d) C_P=4×10^{-1}
(e)
C_P=7.8 10^{-3} at.%
2.5 ± 0.5 nm
(f)
C_P=4 10^{-1} at.%
3.1 ± 1.0 nm
Si-NCs count (at.%)
Si-NCs diameter (nm)
Si-NCs diameter (nm)

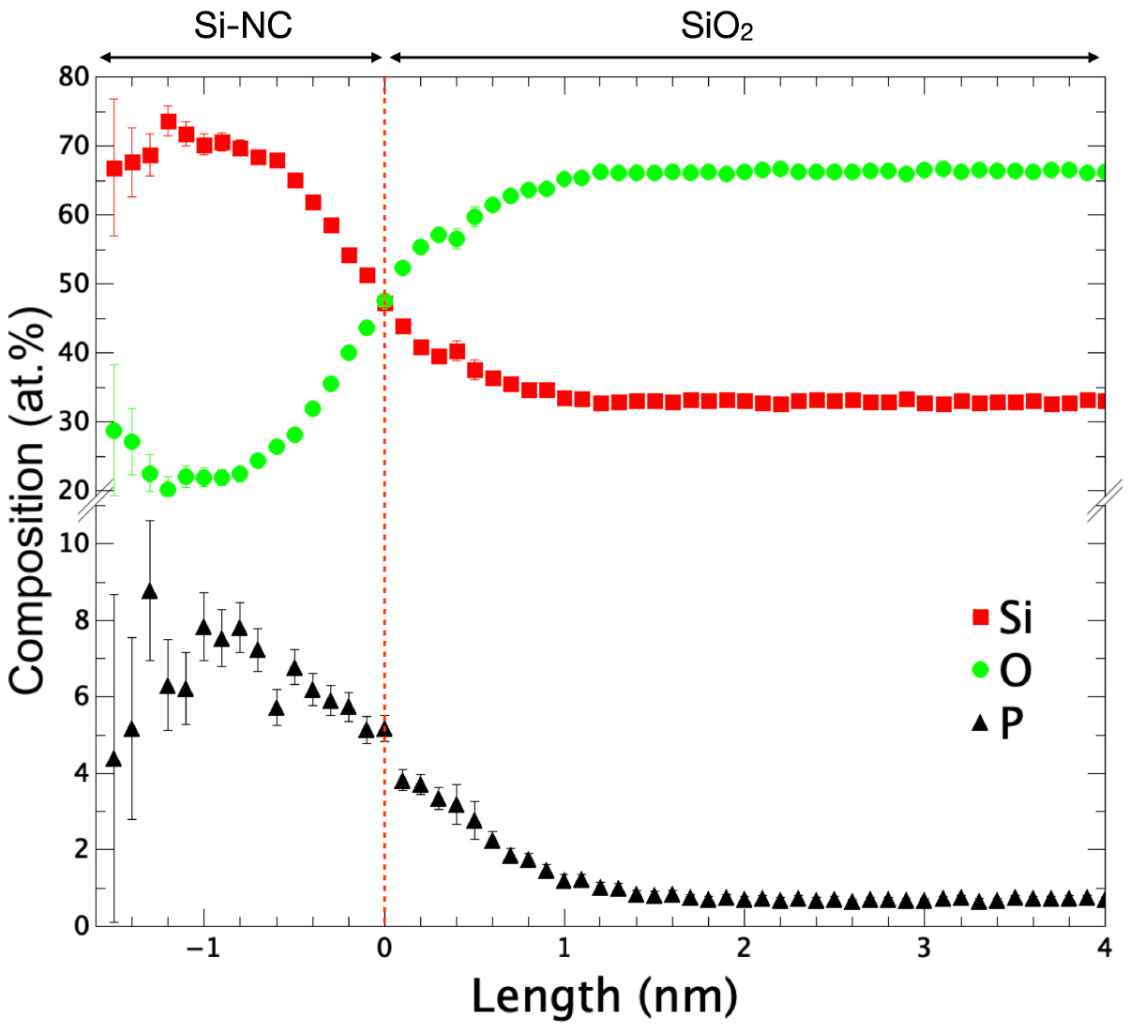
Si-NC
SiO2
Composition (at.%)
Length (nm)
Si
O
P
80
70
60
50
40
30
20
10
8
6
4
2
0
−1
0
1
2
3
4

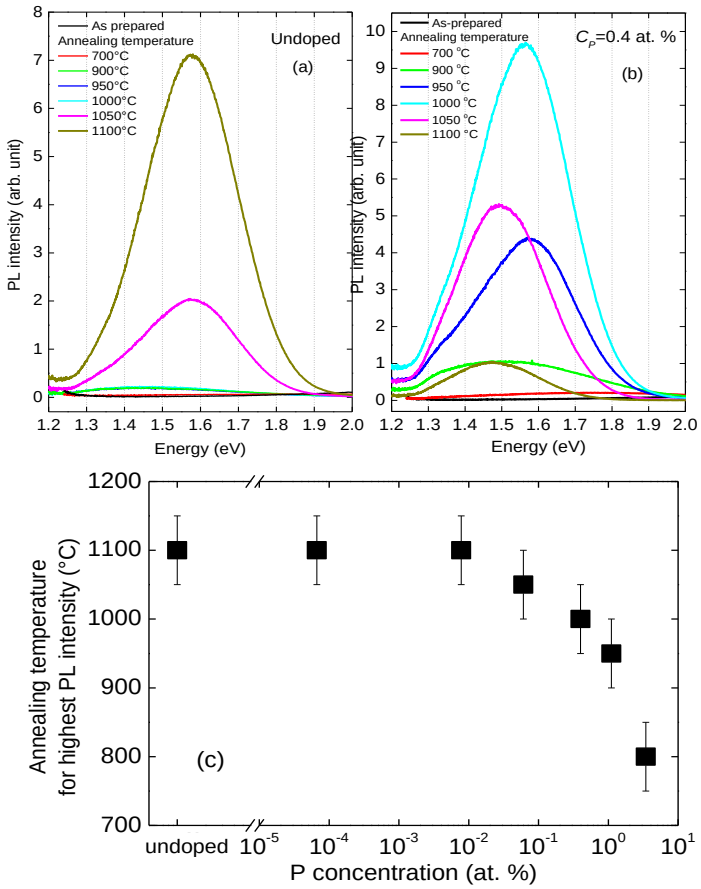
As prepared
Annealing temperature
700°C
900°C
950°C
1000°C
1050°C
1100°C
Undoped
(a)
PL intensity (arb. unit)
Energy (eV)
As-prepared
Annealing temperature
700 °C
900 °C
950 °C
1000 °C
1050 °C
1100 °C
C_P=0.4 at. %
(b)
PL intensity (arb. unit)
Energy (eV)
Annealing temperature for highest PL intensity (°C)
(c)
undoped
P concentration (at. %)

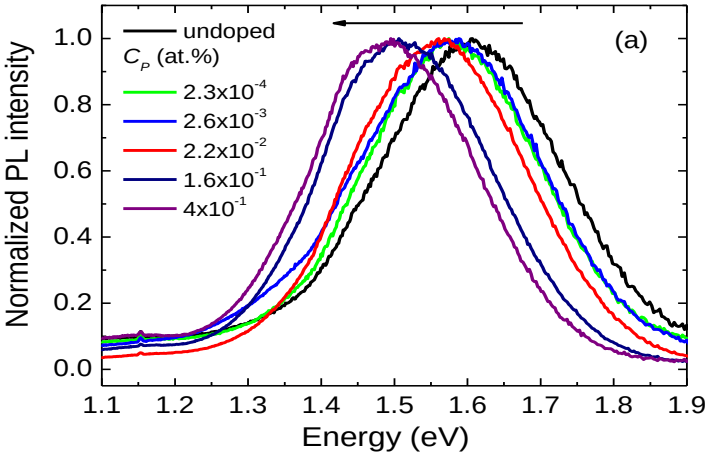
undoped
C_P (at.%)
2.3x10^{-4}
2.6x10^{-3}
2.2x10^{-2}
1.6x10^{-1}
4x10^{-1}
(a)
Normalized PL intensity
Energy (eV)

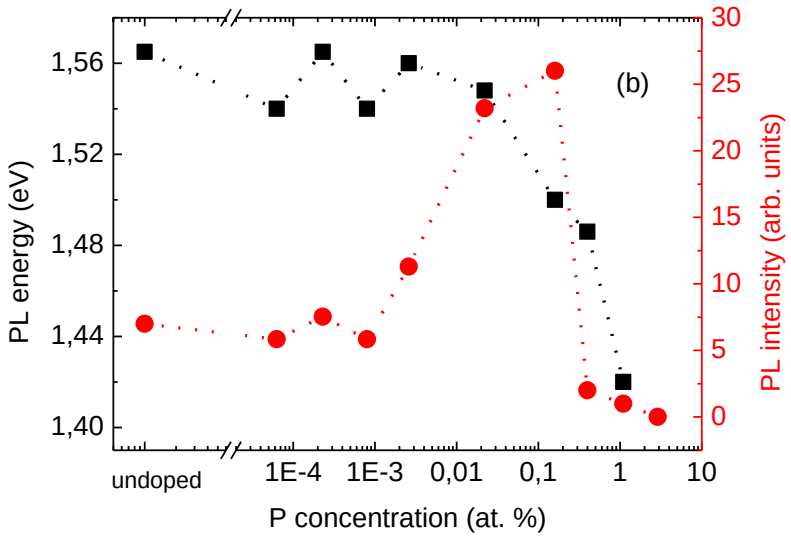
(b)
PL energy (eV)
PL intensity (arb. units)
undoped
1E-4
1E-3
0,01
0,1
1
10
P concentration (at. %)

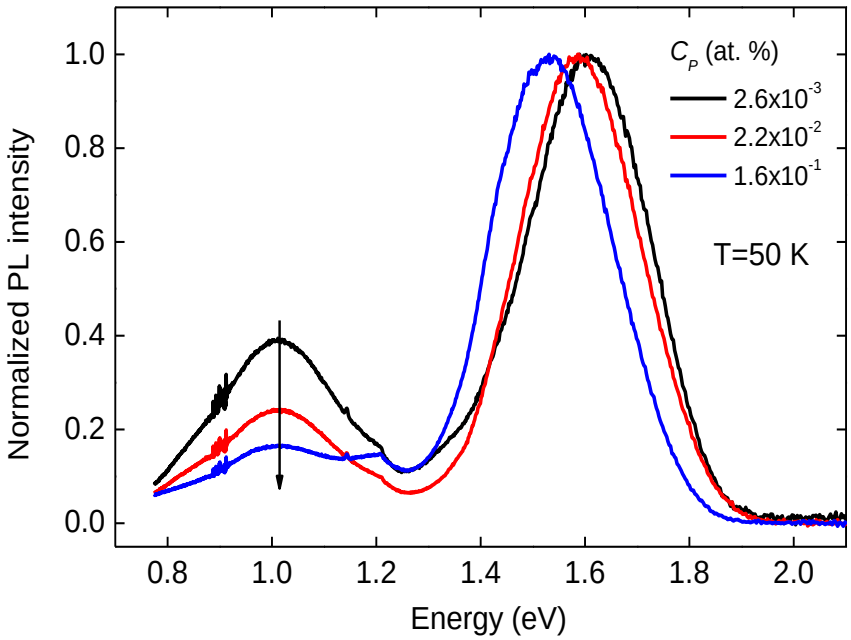
Normalized PL intensity
Energy (eV)
C_P (at. %)
2.6x10^{-3}
2.2x10^{-2}
1.6x10^{-1}
T=50 K
0.0
0.2
0.4
0.6
0.8
1.0
0.8
1.0
1.2
1.4
1.6
1.8
2.0

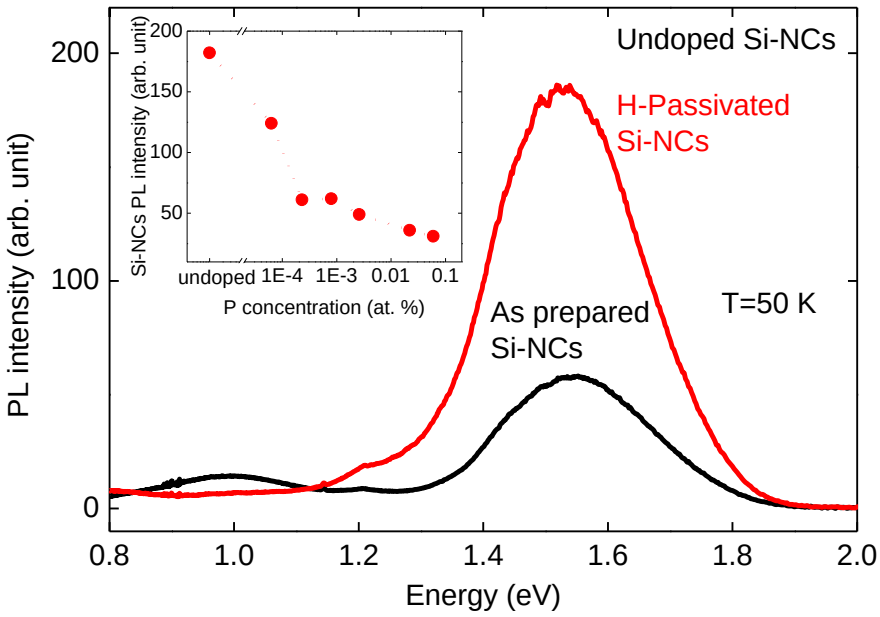
Undoped Si-NCs
H-Passivated
Si-NCs
As prepared
Si-NCs
T=50 K
PL intensity (arb. unit)
Energy (eV)
0
100
200
0.8
1.0
1.2
1.4
1.6
1.8
2.0
Si-NCs PL intensity (arb. unit)
50
100
150
200
undoped
1E-4
1E-3
0.01
0.1
P concentration (at. %)

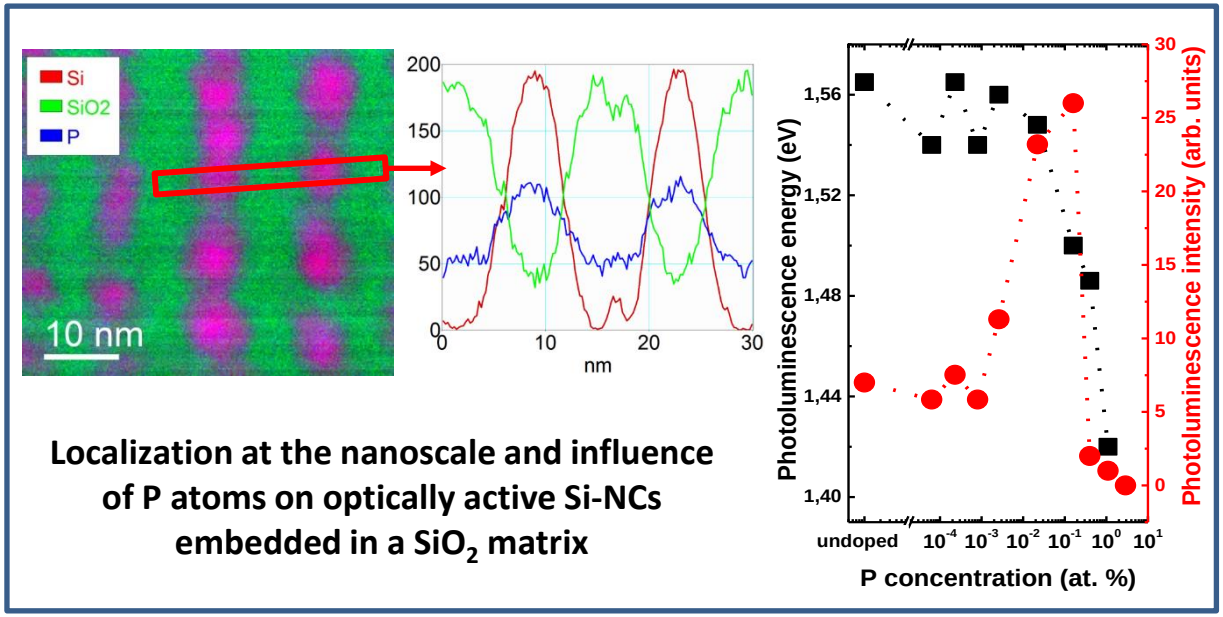

Localization at the nanoscale and influence of P atoms on optically active Si-NCs embedded in a SiO_2 matrix